SAND2011-2474P
SAND#####-##### #

SANDIA NATIONAL LABORATORIES
HYDROGEN PROGRAM STORAGE PROJECTS

QUARTERLY PROGRESS REPORT FOR JULY- SEPTEMBER 2010.

Sandia National Laboratories is a multi-program laboratory managed and operated by Sandia Corporation, a wholly owned subsidiary of Lockheed Martin Corporation, for the U.S. Department of Energy's National Nuclear Security Administration under contract DE-AC04-94AL85000.

TASK 1– IEA/IPHE PARTICIPATION

TASK 1.1 Hydrogen Storage Materials:

Principal Investigator: Mark Allendorf
No participation this quarter.

TASK 2–DEVELOP GENERALIZED METHODS AND PROCEDURES TO INVESTIGATE REACTIVITY PROPERTIES OF HYDROGEN STORAGE MATERIALS (PHASE II)

Principal Investigator: Daniel E. Dedrick

The work planned under this task was competitively selected under DOE solicitation #DE-PS36-06GO96012F. The primary focus of this program is to develop generalized methods and procedures required to quantify the reactivity properties of hydrogen storage materials to enable the design, handling and operation of solids-based hydrogen storage systems. We are performing the experimental and modeling/simulation efforts that are required to understand chemical and physical processes during accident scenarios. Ultimately, this effort identifies and develops hazard mitigation strategies, and provides the technical basis that is required for eventual codes and standards development.

The project is organized into three subtasks:
Subtask 2.1 Quantify contamination chemical processes and hazards (Phase I)
Subtask 2.2 Predict chemical reactions and hazards during accident scenarios (Phase II)
Subtask 2.3 Identify and demonstrate hazard mitigation strategies (Phase II)

Summary of accomplishments in Q4 of FY10:
Explored the effect of polymer cross-linking in polystyrene-sodium alanate composites

- Variation of cross-linking led to different physical properties of the material and only slight differences in hydrogen storage capacity
- Cycling has a dramatic impact on the reactivity of the polystyrene formulations indicating need for a more robust matrix.

SUBTASK 2.3 Identify and demonstrate hazard mitigation strategies

Task contributors: Joe Pratt, Craig Reeder, Joseph Cordaro

COMPOSITE MATERIALS CHARACTERIZATION

Sodium alanate (NaAlH4) with 10% (wt) graphite undergoes a strong exothermic oxidation reaction when exposed to air, which can cause high temperatures and/or fire. Composites, polystyrene cross-linked in the presence of the sodium alanate active material, were investigated as a potential route to reduce the heat generated in an oxidation reaction.

The amount of cross-linking depends on the ratio of the two monomers styrene (sty) and divinylbenene (dvb). A low ratio, such as 1:1 sty:dvb, will result in a highly cross-linked, brittle material. Higher ratios, such as 10:1 sty:dvb, result in less cross-linking and a tougher material. A tough material is promising for practical applications because it is amenable to fabricating as pellets or balls and, if it can remain in this form, provides simpler means of servicing or replacing the hydrogen storage material in a storage tank. Therefore, we decided to expand our investigation to materials with sty:dvb ratios of 20:1, 40:1, and pure styrene.

We found the 40:1 to be the toughest material of the 20:1, 40:1, and pure styrene formulations and also observed some self-healing properties of the 40:1 composite when heated to 200 °C. The degree of polymerization and products of decomposition for the 40:1 composite were consistent with other cross-linking formulations. In all of the composites synthesized, the loading weight percent (16.7%) of polymer was constant, only the sty:dvb ratio was modified. This led us to test the 40:1 composite against more highly cross-linked systems to determine if a tougher material would provide more desirable performance and decomposition characteristics.

Figure 1 shows the dependence of hydrogen storage capacity on material type. This is measured just after initial synthesis, before the material has undergone any cycling. It is apparent that the neat material has a higher initial capacity than any of the materials with polymer added. One reason for this is the substitution of 16.7% of the NaAlH4 with the polystyrene, reducing the amount of active material in the measurement. However, it can also be seen that the capacity changes for the different sty:dvb ratios despite the same amount of polymer being present, and the capacity increases with less cross-linking (higher ratio). This phenomena requires further investigation.

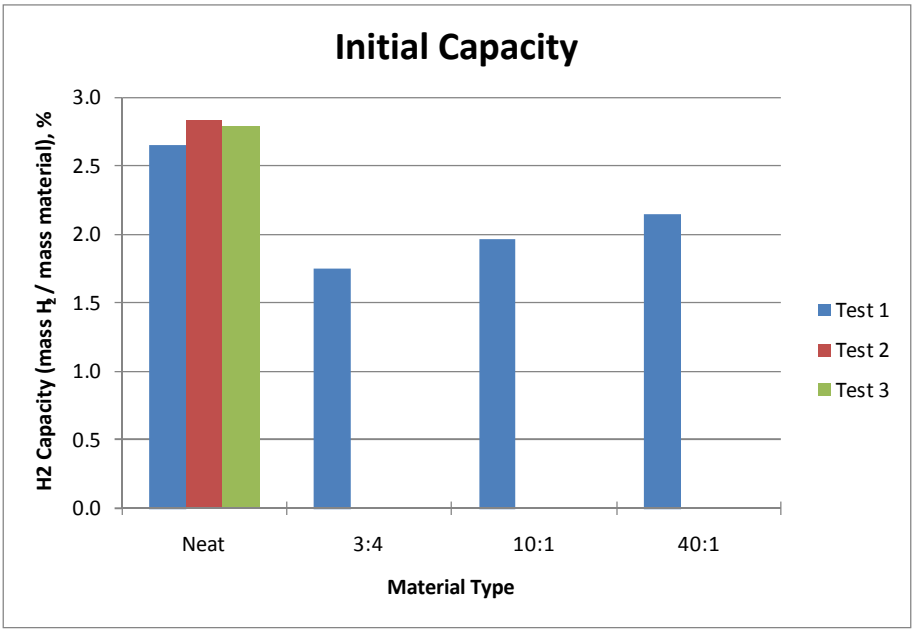

Figure 1: Effect of material type on the initial (uncycled) hydrogen capacity. The addition of polymer reduces the initial capacity, but the higher-ratio materials (lower cross-linking) exhibit less reduction.

Figure 2 shows a clear reduction in capacity upon cycling the material for all of the materials studied and shows some general trends. First, the initial slopes of declining capacity are similar, indicating that the initial reduction in capacity is more a characteristic of the active material than a result of adding polymer. Second, for the long duration tests, the capacity achieves steady state. This indicates that after an initial conditioning period, the performance of a NaAlH4 storage system is predictable over the number of cycles studied.

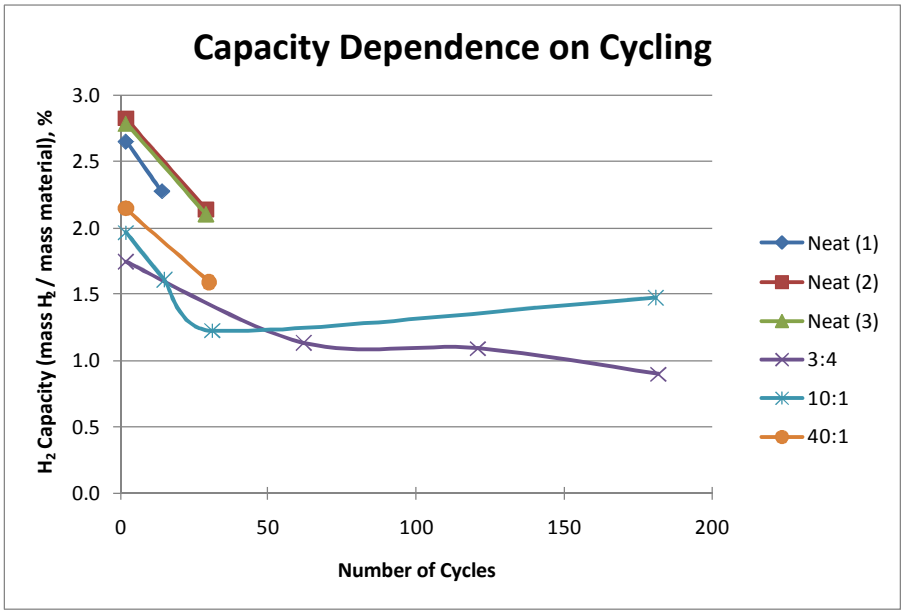

Figure 2: Effect of cycling on hydrogen capacity, for different material sets. The initial reduction in capacity is similar for all materials indicating it may not be an effect of the added polymer but of that of the neat material. There is also a trend towards a stable, steady state upon many cycles.

After hydrogen cycling the composites were analyzed by thermogravimetric analysis (TGA) in order to determine how much polymer remained. Samples exhibiting physical properties from brittle (sty:dvb, 3:4) to tough (sty:dvb, 40:1) were analyzed. From Figure 3, the sample with a sty:dvb ratio of 10:1 retained the highest overall percentage of polymer after 180 cycles, 9.69%. The 1:1 and 10:1 samples both lost 28% of the polymer over the first 30 cycles, whereas the 40:1 sample lost 58%. The erratic results for the 1:1 sample above 30 cycles illustrates the error associated with TGA measurements of cycled material. For the three cycled composites, the cycling performance is best at sty:dvb ratio of 10:1. This corresponds to a balance in the observed mechanical properties of the sample.

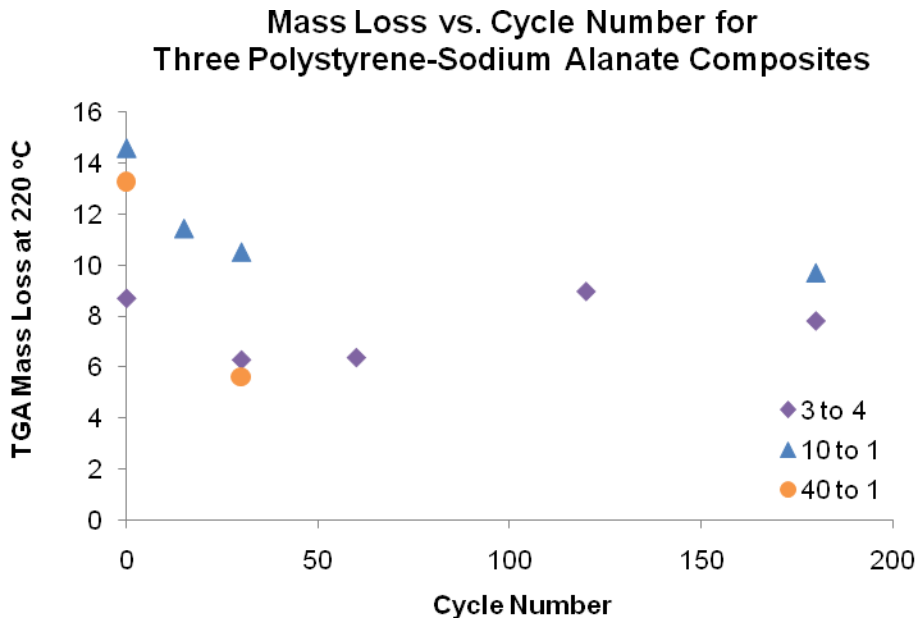

Figure 3. Mass loss versus cycle number for composites of three different styrene:divinylbenzene cross-linking ratios.

A mass spectrometer attached to the TGA instrument allowed us to determine decomposition products of composites before and after cycling at multiple cross-linking ratios. In each sample analyzed, peaks consistent with the masses of toluene and styrene were observed. In most samples, peaks consistent with the mass of divinylbenzene were also observed. The observed reduction in the amount of polymer in the composite with cycling decreases the ability of the composite to mitigate heat release.

Figure 4 shows the hazard mitigation (reduction of heat release) effectiveness of the different options, with comparison to the neat material. Additional heat release upon cycling is seen for the neat material, indicating that additional hydrogen may remain adsorbed onto the active material when it is oxidized. The exact reasons for this phenomenon in the neat is not yet understood and requires further analysis to check if it is a real effect or an artifact of experimental error.

It is clear that addition of the 3:4 polymer is effective at reducing heat release in the uncycled material, but neither the 3:4 or 10:1 additive is effective after cycling. Oxidation of the

polystyrene present in the composites is likely and indicates that polymers containing functionalities other than styrene and divinylbenzene are desirable.

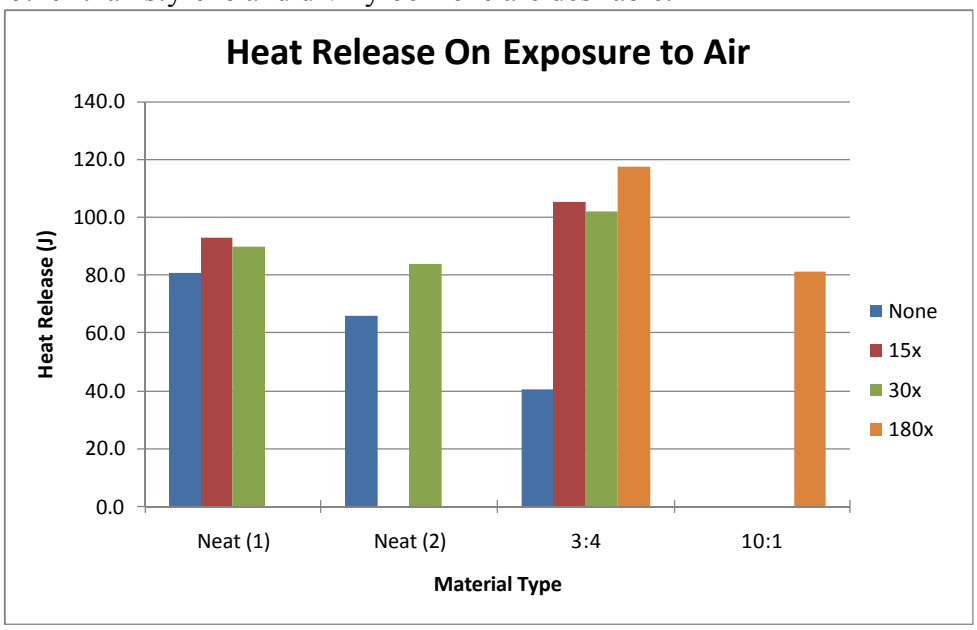

Figure 4: Heat release of the different material sets. While the 3:4 polymer-added material exhibits a mitigating effect (lower heat release compared to the neat material) in the uncycled state, the effect disappears and is perhaps reversed upon cycling.

Figure 5 shows the permeability of the different materials before and after cycling. Two observations can be made from these results. First is that the neat material exhibits little or no change with cycling, while the 3:4 material shows a decrease in permeability. The second is that the permeabilities of the uncycled neat and 3:4 materials are similar. During cycling, the amount of polymer present in the composite slowly decreases, so this result indicates that a more robust polymer system is needed.

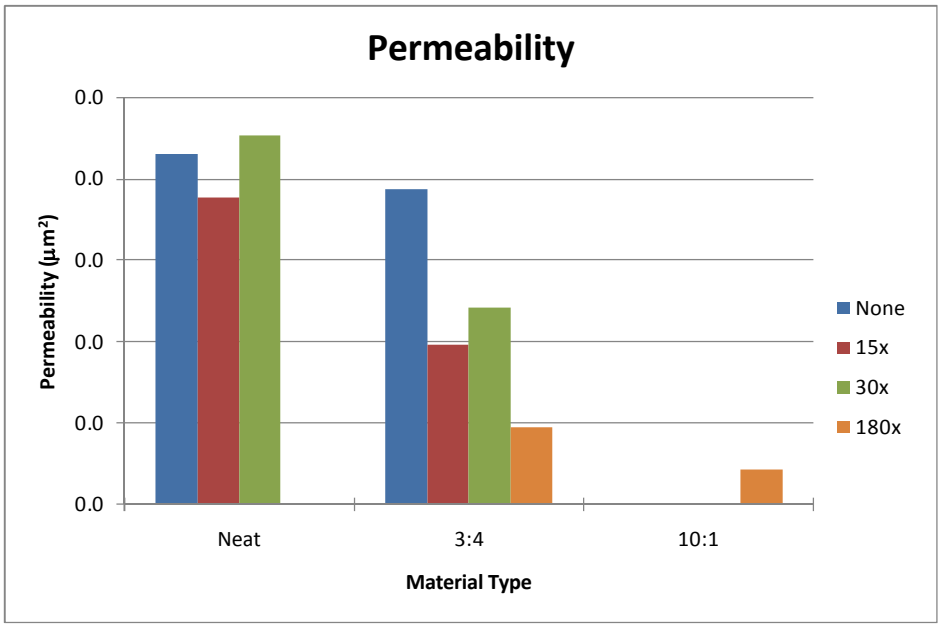

Figure 5: Permeability of the materials before and after cycling. The addition of polymer greatly reduces the permeability of the material upon cycling.

The combination of results from the change in capacity with cycling, and the change in permeability with cycling indicates that the reduction in capacity is not due solely to a reduction in permeability, since the capacity of neat material decreases despite the fact that the permeability does not appreciably change. This reinforces the belief that the reduction in capacity upon cycling is more due to a characteristic of the neat material than an effect of the polymer.

The heat release and permeability data of the 3:4 sample at different cycling states seems to show a correlation between the two: as the permeability decreases, the heat release seems to increase and vice-versa. Physical observations note that the material cycled many times has a much finer powder form than either the same material that has been through fewer cycles or the uncycled material. TGA indicates that the polymer is persistent, but significant amounts volatilize during cycling. The increase in heat release could therefore be due to a change in the materials structure, with more, smaller particles resulting in a higher surface area exposed to oxidation.

MATERIALS SCALE-UP AND NEW MATERIALS SYNTHESIS

This quarter, we scaled up composite reactions and began work on elastomeric, flame-resistant monomers.

Composite reactions with styrene:divinylbenzene (sty:dvb) ratio of 1:1 were carried out under a variety of heating and mixing conditions on scales requiring between 30 g and 305 g of sodium alanate. In these reactions, we were unable to achieve similar degrees of polymerization as those seen on a 6 g scale. This reduced the amount of polymer in the composite, observed as the percent mass loss in thermogravimetric analysis (TGA) heating curves. Figure 6 compares the percent mass loss vs. reaction scale and does not indicate a clear trend in degree of polymerization with the size of the reaction.

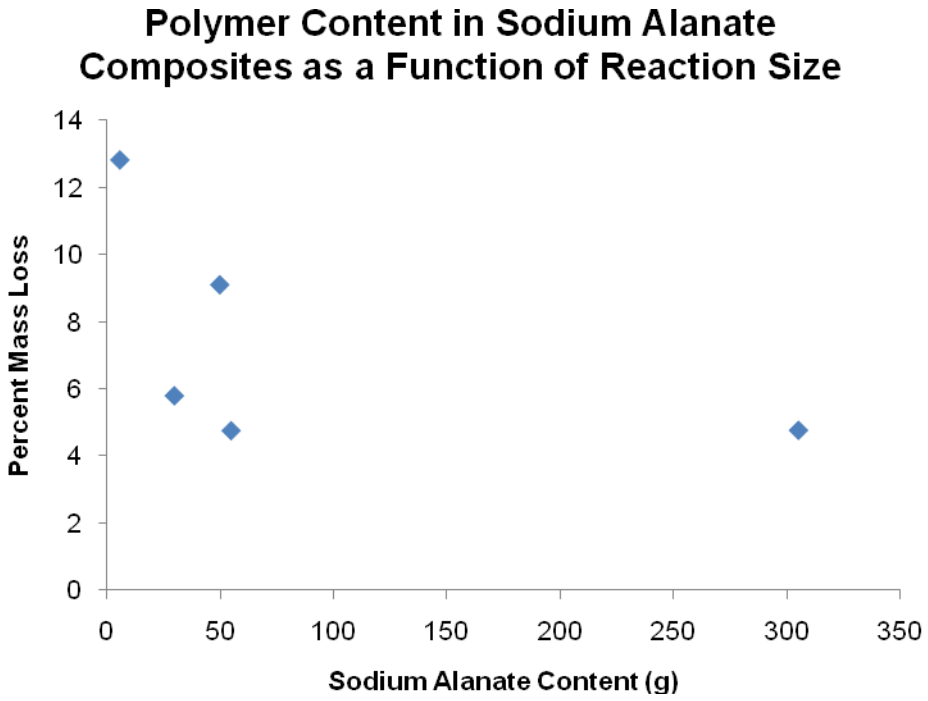

Figure 6. Weight percent polymer vs. sodium alanate content in 1 : 1 styrene : divinylbenzene composites of various reaction sizes. Polymer weight percent was measured as percent mass loss between 200 and 350 °C by TGA.

Elastomeric, siloxane-containing, cross-linking monomers are being explored to improve the mechanical properties, flame-resistant capabilities, and hydrogen cycling of polystyrene-based composites. We are currently exploring two synthetic routes to siloxane-containing cross-linking monomers, compounds **1** and **2** in Figure 7.

1 **2**

Figure 7. The chemical structures of two target siloxane-containing, cross-linking monomers.

In the next quarter, we will finalize the performance characterization of the polystyrene-sodium alanate composites and compile final documentation and reports. In addition, we will use the results from the polystyrene tests to make recommendations for future work including other possible polymer formulations that do and do not include styrene, and are more active at mitigating the heat release.

Publications and presentations

1. Reeder, C.L.; Pratt, J.W.; Cordaro, J.G.; Kanouff, M.P.; Bradshaw, R.W.; Dedrick, D.E. Composite Materials for Solid-State Hydrogen Storage. ACS Sumer School on Green Chemistry and Sustainable Energy, Golden, CO, July 21-29, 2010.

TASK 3–TUNABLE THERMODYNAMICS AND KINETICS FOR HYDROGEN STORAGE

Principal Investigator: Mark Allendorf

TASK 3.2 HYDROGEN SORPTION MEASUREMENTS AND KINETICS

$NaAlH_4$@CuBTC MOF: Global kinetics and analysis of isothermal reaction steps. The release of H_2 from $NaAlH_4$ infiltrated into the 1.3 nm pores of CuBTC is dramatically accelerated, with the desorption temperature (into vacuum) dropping ~ 100 °C. We analyzed the solid state reaction by measuring the H_2 desorption partial pressure at isothermal steps in the temperature range 50-200 °C, using the Simultaneous Thermogravimetric Molecular Beam Mass Spectrometry facility (STMBMS). From these data we can determine whether the system is in equilibrium with the condensed phase. A small alumina type reaction cell, fitted with an alumina style cap assembly having an orifice diameter of 11.1 μm was loaded with the sample and sealed with a viton o-ring. The sample is covered with a baffle to prevent spattering of material onto the orifice.

Three different samples were analyzed in this set of STMBMS experiments: (1) $NaAlH_4$ infiltrated into CuBTC MOF; (2) $TiCl_4$ catalyzed $NaAlH_4$; and (3) pure $NaAlH_4$. For sample (1) the decomposition may be divided into two regions:

- Below the melting point of $NaAlH_4$: most of the H_2 evolves in the first thermal cycle that probes this region. It is characterized by a relatively constant rate of H_2 release for a number of steps in the first heating set as shown in Figure 1. As the temperature approaches the melting point of $NaAlH_4$ (~115 °C), the H_2 release rate rises rapidly as the sample first attains the isothermal temperature and then falls off exponentially.
- The rate of H_2 release during the cooling portion of the first cycle is much less than is observed in the heating portion. This may indicate absence of an equilibrium type of process. In the second portion of the cycle the rate of release of the products at a given temperature is about the same on the heating and cooling portions of the curve. The H_2 desorption steps appear to be relatively constant over a range of different isothermal temperature steps.

We applied 16 different solid-state reaction models, including surface-limited, diffusion-limited, and nucleation-limited models, to obtain an initial global picture of the kinetics. Preliminary results show that the activation energy for hydrogen desorption from $NaAlH_4$@CuBTC is ~ 50 kJ/mol using a second-order reaction model. *This agrees well with the results of Balde et al. (JACS 2008), in which somewhat larger particles (~ 2 nm) displayed an activation energy of 58 kJ/mol. Our results are consistent with increasing destabilization as a function of size and suggest that the chemical environment, which is very different for the MOF and porous carbons used by Balde et al., is not the rate-determining factor.* Preliminary results for sample (2) indicate desorption is at equilibrium, but sample (3) displays irregular behavior suggestive of a diffusion-limited mechanism. This analysis will be completed next quarter.

$LiBH_4$ infiltration of nanoporous carbons. The decomposition behavior of $LiBH_4$ was investigated in the presence of highly ordered nanoporous carbon (NPC) with columnar pores of average pore diameter 2.0 nm and a narrow size distribution. The XRD pattern of the pre-melted $LiBH_4$@NPC did not show the Bragg peaks of $LiBH_4$ indicating $LiBH_4$ became amorphous after it was confined in the nanopores of NPC through melt infiltration. The diffraction peaks of $LiBH_4$ still exist in the pre-melted sample of $LiBH_4$@carbon aerogels indicating the existence of crystalline $LiBH_4$ in this nano-composite system. In contrast to previous studies of $LiBH_4$ confined in 12 nm and larger carbon aerogel pores, the non-crystalline $LiBH_4$ embedded in 2.0 nm pores not only results in the disappearance of the structural phase transition at around 100°C, and the melting transition, but also the significant decrease of the onset desorption temperature from 460°C to 220°C. More importantly, the formation of B_2H_6 both in bulk $LiBH_4$ and samples of NPC powders infiltrated with $LiBH_4$ using two different methods have been characterized. Diborane release is suppressed or eliminated in the decomposition of non-crystalline $LiBH_4$ in the 2.0 nm pores, and only forms during the infiltration process. Tightly confining nano-framework materials may therefore mitigate both safety concerns and loss of active material in borohydride-based hydrogen storage systems. In comparison to the large pore size and the broader size distribution of carbon aerogels (25 nm), the NPC 2.0 nm pore size and narrow size distribution are likely responsible for the non-crystalline $LiBH_4$ in our carbon. Figure 3 shows the nitrogen sorption isotherms of ***$LiBH_4$@NPC.*** S_{BET} and the total pore volume of ***$LiBH_4$@NPC*** were reduced to 116 m^2/g and 0.09cm^3/g, respectively, indicating the filling or blocking of the pores by $LiBH_4$. Calorimetry of these samples indicates filling and rules out simple blocking of the pores. The existence of $[BH_4^-]$ in the pre-melted sample was confirmed by means of Fourier transform infrared spectroscopy.

Figure 4 shows the DSC plots of bulk $LiBH_4$, a physical mixture of $LiBH_4$/NPC, and $LiBH_4$@NPC. In agreement with bulk $LiBH_4$ the DSC plot of the physical mixture of $LiBH_4$/NPC shows the orthorhombic to hexagonal structure transition at a temperature of 115°C and melting at 284°C. The decomposition peak of bulk $LiBH_4$ appears around 495°C. Rapid dehydrogenation after the melting was observed for $LiBH_4$/NPC, and the decomposition peak appeared around 345°C. In contrast, the pre-melted sample of $LiBH_4$@NPC did not show the structure transition from orthorhombic to hexagonal and no distinct melting point was observed, indicating that $LiBH_4$ confined in NPC becomes amorphous. $LiBH_4$@carbon aerogel has a lower, but distinct melting point. We speculate this may be due to lattice strain induced via an interaction between the $LiBH_4$ and the carbon surface. In contrast, from the DSC curve of ***$LiBH_4$@NPC we can see that $LiBH_4$ confined in NPC begins to decompose*** **below** ***the normal melting point.***

To examine the decomposition pathway, we have observed gaseous decomposition products of bulk $LiBH_4$, a physical mixture of $LiBH_4$/NPC, and pre-melted samples of $LiBH_4$@NPC, using a direct line-of-site residual gas analyzer and mass spectrometer (RGA-MS). It is observed in the MS of bulk $LiBH_4$, and the sample of physically mixed $LiBH_4$/NPC, that the decomposition results in the formation of B_2H_6 as shown in Figure 5. B_2H_6 release data of bulk $LiBH_4$, the physical mixture of $LiBH_4$/NPC, and the pre-melted $LiBH_4$@NPC were taken at 410***, 325, and 382°C, respectively.*** Interestingly, for the physically mixed sample of $LiBH_4$/NPC, B_2H_6 formed during the initial decomposition of $LiBH_4$ but for the bulk sample B_2H_6 was mainly observed *after* significant release of H_2. More interestingly, B_2H_6 is not indicated in the pre-melted sample of $LiBH_4$@NPC.

Our results indicate that the carbon framework may prevent the formation of B_2H_6 and the decomposition pathway is altered by the presence of the framework through size confinement and/or surface interaction effects as evidenced by the wetting behavior. Alternatively, it may suggest that $LiBH_4$ decomposing from a non-crystalline state cannot produce B_2H_6.

TASK 3.3 THEORETICAL MODELING FOR RATIONAL DESIGN OF PARTICLES

Subtask 3.3.1 (UMSL)

Phase diagram of nano-cluster $NaAlH_4$ from first-principles DFT and nano-PEGS cluster prototypes. A preliminary phase diagram for nano-cluster $NaAlH_4$, up to 8 formula units of the decomposition products, is shown in Figure 2. Decomposition products included 1-8 formula units of $NaAlH_4$, Na, Al, NaAl, NaH, and AlH_3. Na_3AlH_6 was excluded based on the instability of these clusters. All non-metallic clusters were generated using the PEGS method. The Gibbs free energy for the set of clusters was minimized for a given temperature and pressure to find the clusters present at a given Al:Na ratio.

While the decomposition pathway depends on the Na:Al ratio, for a ratio of 1, we find the decomposition pathway for $NaAlH_4$ clusters is single step into AlNa, mixed metal clusters. The $NaAlH_4$ clusters increase in stability with decreasing size. The lowest temperature reaction pathways were for very small Na clusters, which were unstable below n=3, where the ground state was metallic Na and H_2 gas. A manuscript including more detailed results is in preparation.

Table 1. Decomposition enthalpy for clusters of $NaAlH_4$. Cluster geometries were generated using the PEGS method. Enthalpies include finite temperature entropy contributions and were calculated using first-principles DFT.

T [°C]	ΔH [kJ/mol H_2]	
597	147.82	$(NaAlH_4)_1 \rightarrow (AlNa)_1 + 2.0\ H_2$
435	115.12	$(NaAlH_4)_2 \rightarrow (AlNa)_2 + 4.0\ H_2$
350	101.38	$(NaAlH_4)_3 \rightarrow (AlNa)_3 + 6.0\ H_2$
326	97.20	$(NaAlH_4)_4 \rightarrow (AlNa)_4 + 8.0\ H_2$
239	81.41	$(NaAlH_4)_5 \rightarrow (AlNa)_5 + 10.0\ H_2$
237	80.60	$(NaAlH_4)_6 \rightarrow (AlNa)_6 + 12.0\ H_2$
222	76.91	$(NaAlH_4)_7 \rightarrow (AlNa)_7 + 14.0\ H_2$
231	79.79	$(NaAlH_4)_8 \rightarrow (AlNa)_8 + 16.0\ H_2$

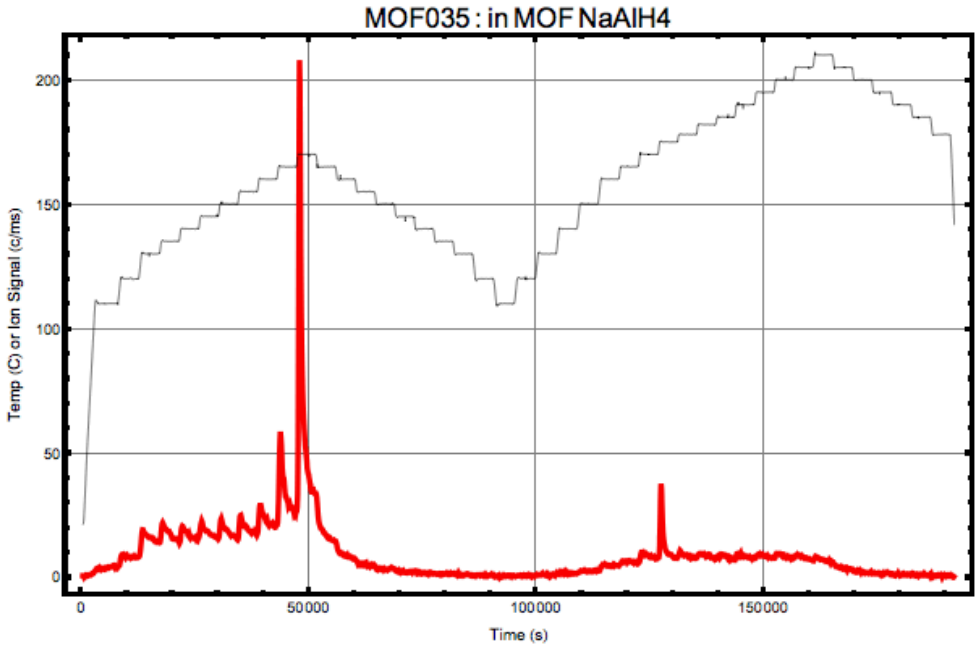

Figure 1. Isothermal reaction steps for the desorption of hydrogen from $NaAlH_4$@CuBTC. Two desorption regions are observed, the first one during the heating, leading up to the melting of $NaAlH_4$ and the other during the cooling off period.

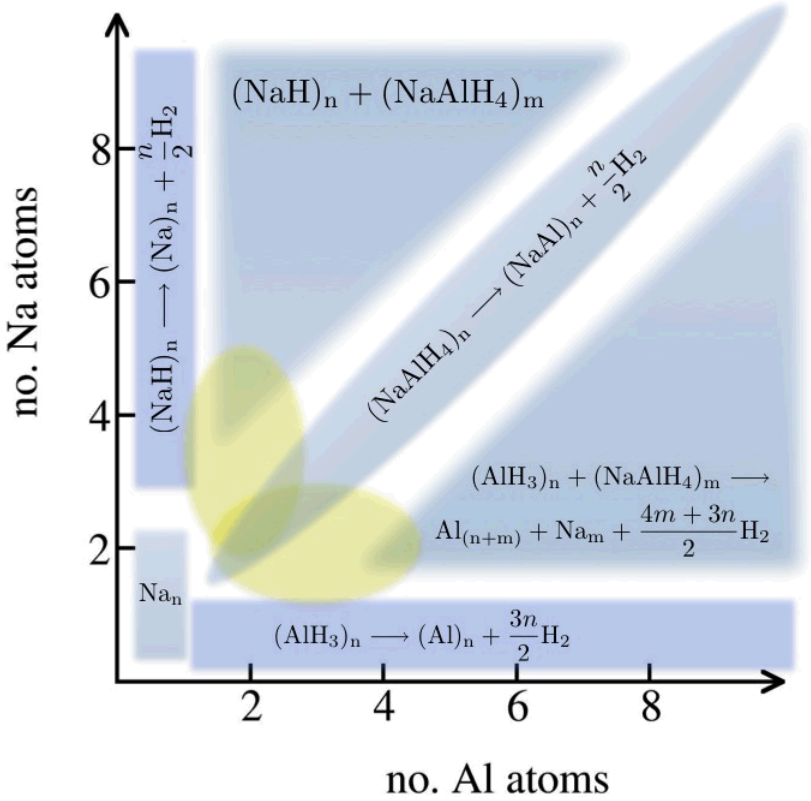

Figure 2. Preliminary phase diagram for small clusters of Na-Al-H.

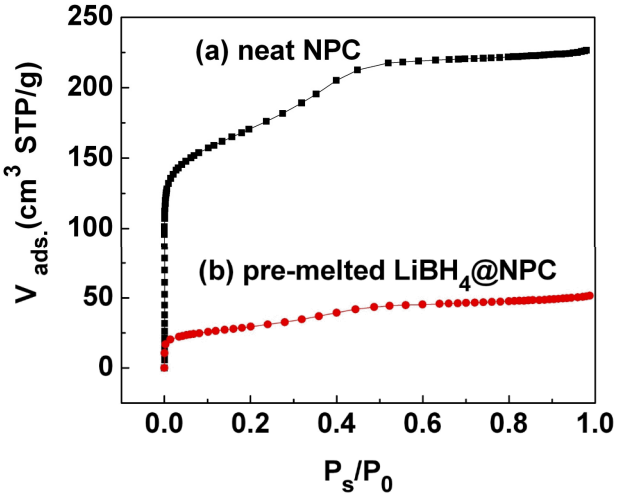

Figure 3. Nitrogen sorption isotherms of (a) NPC with a surface area and pore volume of 594m^2/g, and 0.35 cm^3/g respectively, and (b) pre-melted $LiBH_4$@NPC, with a surface area and pore volume of 116 m^2/g and 0.09 cm^3/g, indicating that $LiBH_4$ has infiltrated the pores.

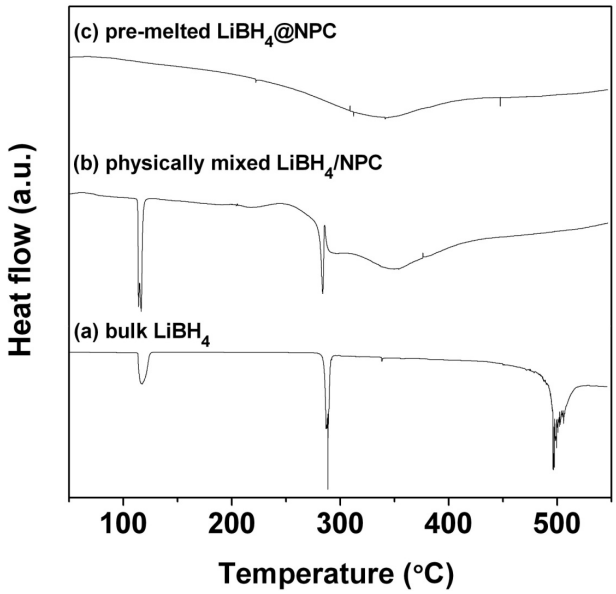

Figure 4. ***DSC traces of (a) bulk $LiBH_4$, (b)*** physically mixed $LiBH_4$/NPC***, and (c) pre-melted $LiBH_4$@NPC. The heating rate was 10°C/min.***

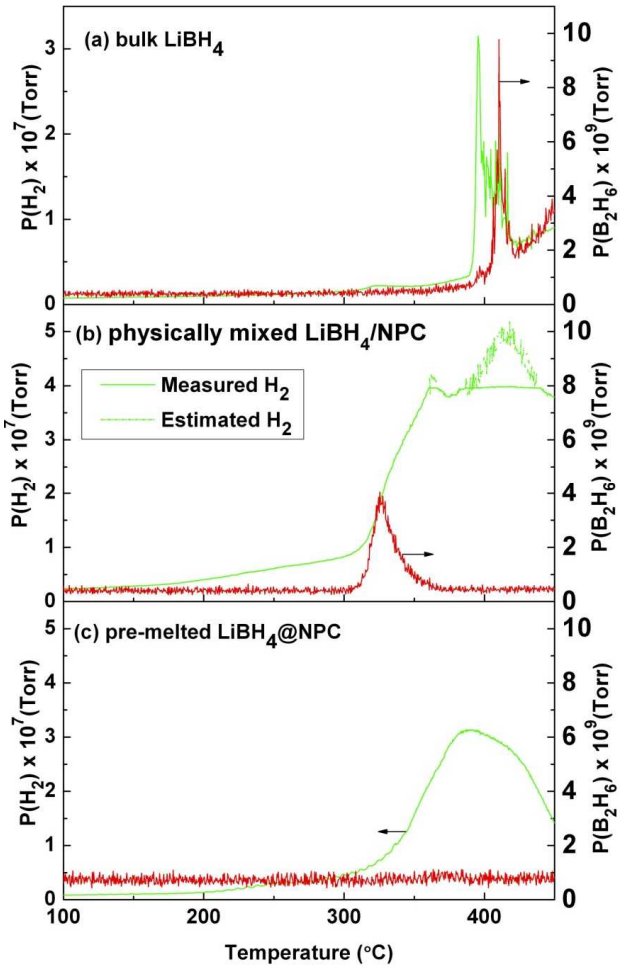

Figure 5. B_2H_6 and H_2 release with increasing temperature for (a) bulk $LiBH_4$, (b) physically mixed $LiBH_4$/NPC, and (c) pre-melted $LiBH_4$@NPC. The release of diborane is absent in the pre-melted LiBH4@NPC sample. The H_2 partial pressure exceeded the RGA tolerance in the physical mixture of $LiBH_4$/NPC. The estimation of partial pressure above the flat green segment is based on the linear relationship between the partial pressures of m/z=1 and m/z=2.

Subtasks 3.3.2 and 3.3.3 (UCB/MIT/Sandia).

Diffusion Monte Carlo (DMC) modeling of Li and LiH clusters: comparisons with Wulff Construction model. DMC was previously shown by us to be very accurate for MgH_2 clusters (Wu, Allendorf, and Grossman. *J. Amer. Chem. Soc.* **131** (2009), 1391). In that investigation we found that DFT exhibits substantial non-systematic errors with respect to DMC and obtain similar results here. For $(LiH)_n$ and $(Li)_n$ clusters, we extrapolated the cluster binding energies from n = 1 to 20, using the clusters with $n \geq 12$ with the function $E(n) = E(\text{bulk}) + an^{-1/3}$ (Figure 6). This produced a good fit for the larger clusters, which we then used to obtain a smooth curve for the hydrogen absorption energy. Less accurate results obtained from Hartree-Fock and several DFT functional (Figure 7) exhibit non-systematic errors, as in the case of MgH_2 clusters. In particular, at small sizes these methods predict on the one hand stabilization (the PBE GGA functional) to destabilization (Hartree-Fock).

Comparing the DMC predictions to the results of Kim et al. obtained from a Wulff construction (Figure 8), we find that DMC predicts very little change in the hydrogen absorption energy over most values of n,

with only LiH and $(LiH)_2$ destabilized relative to bulk. In contrast, the Wulff construction predicts that LiH is *stabilized* as its particle radius decreases below~ 9 nm. In fact, of the hydrides examined by Kim et al., only MgH_2 and NaH are predicted to be destabilized at the nanoscale. Our previous DMC results for MgH_2 are consistent with this, although the destabilization occurs at much small particle sizes (< 1 nm diameter). These results suggest that size affects the energetics of hydride nanoparticles only at extremely small sizes. The corollary, however, is that altered chemistry of hydrides, in particular a change in the thermodynamics observed by the group of de Jongh et al. (J. B. Gao et al. *J. Phys. Chem. C* **114** (2010), 4675), but also changes in desorption and adsorption kinetics observed by several groups, are connected in some way to the local chemical environment of the scaffold pores.

Equillibrium composition of LiH-LiH+C systems using FactSage code. We computed the equilibrium composition for pure LiH and (1 mole LiH + 1 mole C) using FactSage, a free-energy minimization code for modeling complex phase equilibria. For pure LiH the calculations predict that at 1 atm LiH first melts at 962 K, then decomposes (Fig. 9A). At 0.001 atm, however, no detectable amounts of liquid LiH are predicted to exist, while the decomposition temperature of $LiH_{(s)}$ is 839 K (Fig. 9B). For the LiH+C system a chemical reaction is predicted to occur to form Li_2C_2, H_2 and small amounts of CH_4. At 1 atm this reaction is predicted to start at 821 K (Fig. 9C), while at 0.001 atm the temperature is as low as 608 K (Fig. 9D). The high-temperature (around 500 °C) formation of Li_2C_2 was reported experimentally in the ball-milled LiH-carbon composites. Experiments are currently underway to determine the identity of the reaction products. As far as CH_4 formation is concerned, significant amounts of this gas were not detected in STMBMS experiments, suggesting that its formation is kinetically limited.

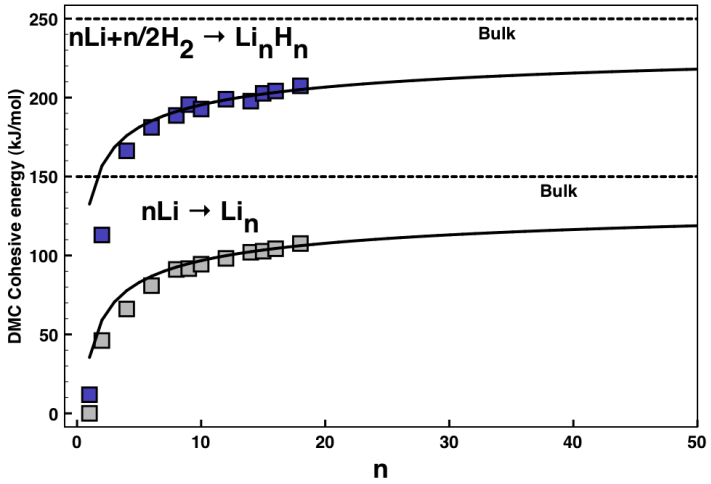

Figure 6. The cohesive energy per formula unit for LiH and Li metal clusters. The results for bulk Li and LiH are also shown (predicted by DMC), as well as an $n^{-1/3}$ extrapolation.

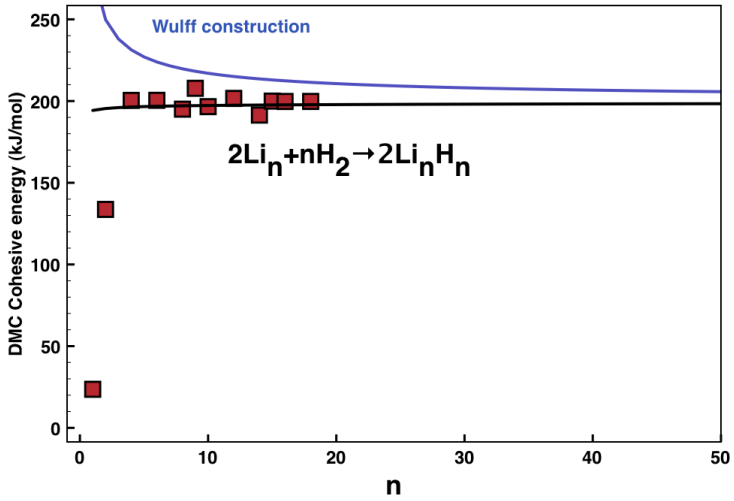

Figure 7. Energy per H_2 molecule gained by transforming Li metal to the hydride, along with the same calculated from the $n^{-1/3}$ extrapolation shown in Figure 8. The results from the Wulff construction are shown as well and are referenced to the value for bulk predicted by DMC.

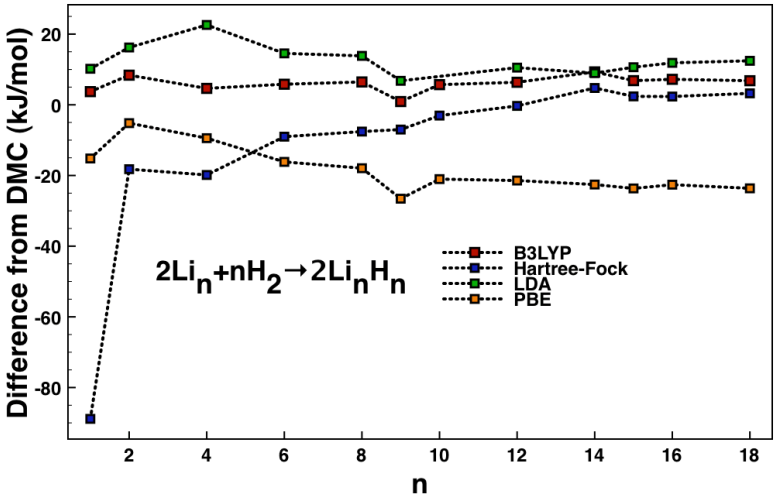

Figure 8. Errors in various density functional theories relative to the DMC results for the Li vs. LiH energy difference.

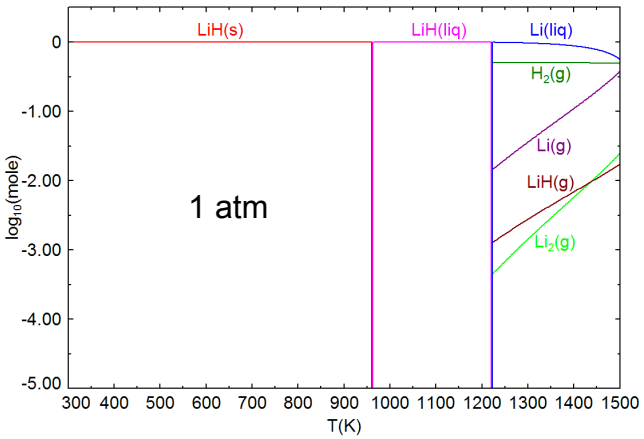

(Fig.9A)

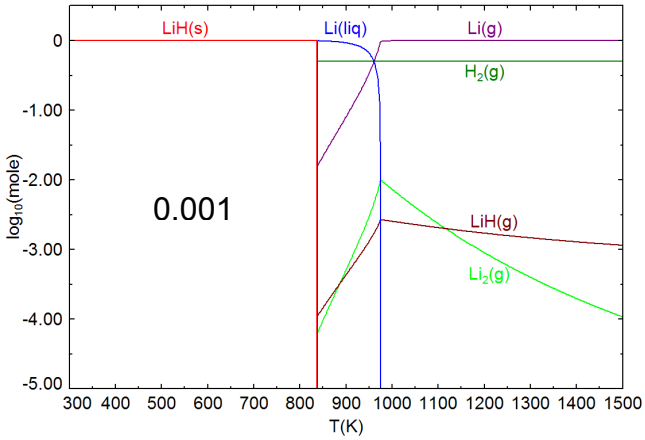

(Fig. 9B)

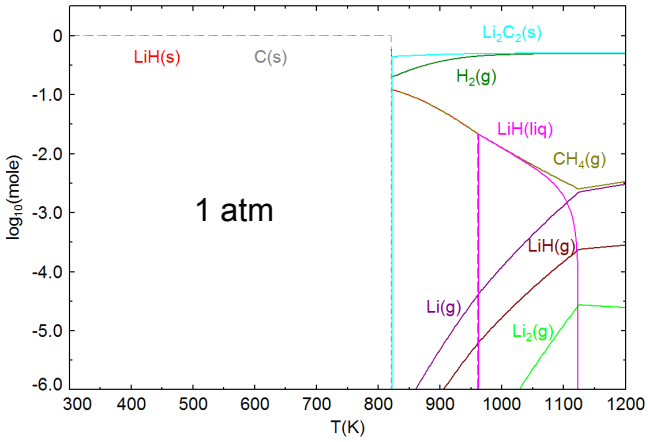

(Fig. 9C)

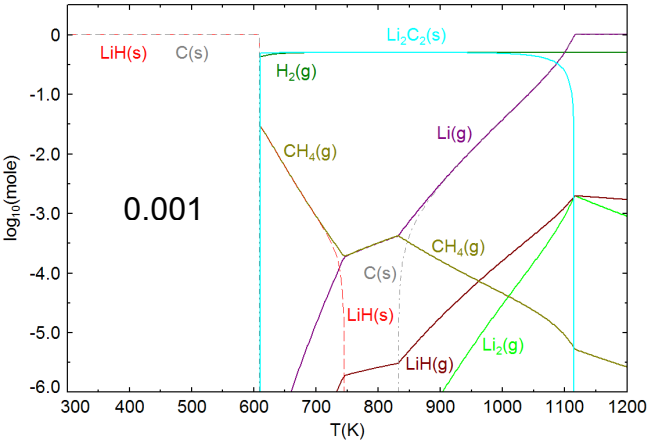

(Fig. 9D)

Figure 9. Predicted equilibrium composition of LiH at 1 atm (Fig.4A) and 0.001 atm (Fig. 4B). Predicted equilibrium composition of LiH+C at 1 atm (Fig. 4C) and 0.001 atm (Fig. 4D).

TASK 7– COLLABORATIVE WEBSITE SUPPORT (STORAGE CENTERS & PROJECTS SHAREPOINT)

Authors: Jennifer Rodriguez and Lynde Farhat

At the request of DOE, Sandia National Laboratories developed the Storage Centers & Projects QuickPlace in May 2005 for the purpose of sharing information in a secure environment among Hydrogen Storage colleagues and partners. The folders maintained within the website provide dated records of documents posted by various participants of the group. As of December 31, 2008 QuickPlace ceased to exist on the Sandia server and was replaced with SharePoint. All data has been transferred from the original QuickPlace, and previous members have access to the new SharePoint site. We will continue to maintain the membership list as approved by DOE and to provide posting services upon request for the restricted member private rooms: (1) DOE Hydrogen Storage (default all), (2) Center Leads and (3) SSAWG. This quarter we have been working on switching to an external network to house the H2 Storage SharePoint. The benefit of using an external network will allow a simpler and shorter process to add new members as well as avoiding the training requirements that Sandia's server was requiring. The files have all been converted to the new website and members will be sent their new log on information next quarter.

Jennifer Rodriguez (jenrodr@sandia.gov) maintains the website and membership list, acts as webmaster between SharePoint Administrators (technical support group) and the DOE Hydrogen Storage Program SharePoint members; providing posting services upon request. Lynde Farhat (lfarhat@sandia.gov) is the point of contact for DOE and room managers for membership authorizations, training and any other concerns.